

Experimental observations of pressure oscillations and flow regimes in an analogue volcanic system

Stephen J. Lane,¹ Bernard A. Chouet,² Jeremy C. Phillips,³ Phillip Dawson,² Graham A. Ryan,¹ and Emma Hurst¹

Abstract. Gas-liquid flows, designed to be analogous to those in volcanic conduits, are generated in the laboratory using organic gas-gum rosin mixtures expanding in a vertically mounted tube. The expanding fluid shows a range of both flow and pressure oscillation behaviors. Weakly supersaturated source liquids produce a low Reynolds number flow with foam expanding from the top surface of a liquid that exhibits zero fluid velocity at the tube wall; i.e., the conventional "no-slip" boundary condition. Pressure oscillations, often with strong long-period characteristics and consistent with longitudinal and radial resonant oscillation modes, are detected in these fluids. Strongly supersaturated source liquids generate more energetic flows that display a number of flow regimes. These regimes include a static liquid source, viscous flow, detached flow (comprising gas-pockets-at-wall and foam-in-gas annular flow, therefore demonstrating strong radial heterogeneity), and a fully turbulent transonic fragmented or mist flow. Each of these flow regimes displays characteristic pressure oscillations that can be related to resonance of flow features or wall impact phenomena. The pressure oscillations are produced by the degassing processes without the need of elastic coupling to the confining medium or flow restrictors and valvelike features. The oscillatory behavior of the experimental flows is compared to seismoacoustic data from a range of volcanoes where resonant oscillation of the fluid within the conduit is also often invoked as controlling the observed oscillation frequencies. On the basis of the experimental data we postulate on the nature of seismic signals that may be measured during large-scale explosive activity.

1. Introduction

Hydrothermal and magmatic flows are frequently two-phase mixtures of gas and liquid, often with solid particles present. These flows generate pressure oscillations that result in measurable vibrations of the ground [e.g., Chouet, 1985, 1986, 1988, 1996a; Chouet *et al.*, 1994; Hurst and Sherburn, 1993; Julian, 1994; Schlindwein *et al.*, 1995; Kumagai and Chouet, 1999, 2000]. If the magmatic activity intersects the surface, then atmospheric vibrations are also generated [e.g., Morrissey and Chouet, 1997a; Garcés *et al.*, 1998]. The source mechanisms inferred from very long-wavelength seismic data yield information about the location, geometry, and orientation of the conduit and the space-time history of the motion of the conduit wall, which is related to the pressure field in the fluid [e.g., Ohminato *et al.*, 1998]. Pressure transients and sustained pressure fluctuations within the conduit [e.g., Chouet, 1996a] are considered to generate long-period (LP) seismicity and harmonic tremor, respectively. Tremor spectra generally fall into two broad categories: multiple peaks at unrelated frequencies associated with path and/or site effects; or one dominant peak, perhaps with

harmonics, usually associated with source resonance [Hurst and Sherburn, 1993; Chouet, 1996a]. Another form of seismicity, known as eruption signal, generally accompanies explosive surface activity and varies greatly in amplitude and duration [Harlow *et al.*, 1996]. The mechanisms generating eruption signals are unknown, but are currently being investigated using computer-based models [Nishimura and Chouet, 1998].

LP events and tremor can occur during preeruption and posteruption periods and during explosive volcanic events. These oscillations have been attributed, among other mechanisms, to the resonance of acoustically discrete sections of the conduit system [e.g., Chouet, 1985, 1986, 1988, 1992; McNutt, 1986]. The source of the pressure transients triggering the resonance remains elusive but may be due to nonlinear excitation within an unsteady flow [Julian, 1994; Chouet, 1996b] or the jerky extension of a crack tip [Aki *et al.*, 1977; Chouet, 1986]. The occurrence of unstable shock waves during flow through a constriction has also been proposed as a source [Morrissey and Chouet, 1997a]. It is also known that individual bubbles resonate at characteristic frequencies. This observation may be used to obtain bubble size distributions and bubble number density [Pandit *et al.*, 1992] in bubbly water jets. These oscillations are thought to be stimulated by flow turbulence and are therefore most likely to occur in inviscid flows such as aerated water rather than in much more viscous magmatic rhyolite foams. Clouds of bubbles are also known to resonate at characteristic frequencies [Lu *et al.*, 1990].

Eruptions also produce continuous acoustic signals with frequencies ranging from 0.001 to 20 Hz and above. These airborne signals can often be correlated with pressure fluctuations and resonance within the volcanic conduit during eruption [Morrissey and Chouet, 1997b; Garcés and McNutt, 1997; Garcés, 1997; Garcés and Hansen, 1998; Garcés *et al.*, 1998].

¹Department of Environmental Science, Lancaster University, Lancaster, England, United Kingdom.

²Volcano Hazards Team, U. S. Geological Survey, Menlo Park, California.

³Centre for Environmental and Geophysical Flows, School of Mathematics, University of Bristol, Bristol, United Kingdom.

Copyright 2001 by the American Geophysical Union.

Paper number 2000JB900376.
0148-0227/01/2000JB900376\$09.00

Pressure oscillations in two-phase flows have been observed experimentally in low-viscosity water-gas systems [e.g., *Leet*, 1988] and attributed to resonance of the gas-filled cavity. Water-CO₂ systems have also demonstrated pressure oscillations (E. Brodsky, personal communication [1998], with reference to *Mader et al.* [1997]). Slow-decompression corn syrup experiments with water as a volatile species [*Hammer et al.*, 1998] showed that pressure oscillations can be attributed to the interaction between nonequilibrium degassing and gas removal rates in higher-viscosity systems. For a given timescale, higher-viscosity liquids allow a greater degree of dissolved gas supersaturation before bubble formation and gas escape, resulting in a pressure rise in the system. This implies that systems far from equilibrium may be particularly prone to oscillatory behavior due to nonlinear interactions between pressure, dissolved gas content, and the degree of supersaturation required for different modes of gas escape [*Phillips et al.*, 1995]. Acoustic vibrations naturally result from unsteady flow and interactions with structures immersed in the flow [*Howe*, 1998]. Pressure oscillations appear to accompany many gas-liquid flows, and considerable efforts are made to suppress such oscillations in industrial applications [*Tong and Tang*, 1997]. The measurement and characterization of pressure oscillations are therefore vital to bridging the gap between laboratory fluid dynamic simulations of volcanic conduit flow, theoretical conduit flow models, and seismoacoustic field measurements. In this study we present data on pressure oscillations measured in expanding foam flows generated by decompression of gum rosin-organic solvent solutions [*Phillips et al.*, 1995].

2. Comparing Experimental and Natural Systems

The laboratory fluid in our experiments has been described by *Phillips et al.* [1995] and uses solutions of natural pine resin (gum rosin) [*Cobbold and Jackson*, 1992] and organic solvents as a hydrated magma analogue. Decompression of a hydrated magma below the water exsolution pressure results in the nucleation and growth of bubbles and the generation of an expanding foam flow in a volcanic conduit [e.g., *Massol and Jaupart*, 1999; *Melnik*, 2000]. Similarly, decompression of the experimental gum rosin-organic solvent solution below the solvent exsolution pressure (≈ 20 kPa for acetone and 60 kPa for diethyl ether at 20°C) forms an expanding foam flow in a vertical cylindrical glass tube (Plate 1). To assess the suitability of this system as an analogue to volcanic conduit processes, we must consider whether the system behavior and the balance of forces acting on the flowing fluid are similar at natural and laboratory scales.

2.1. Geometric Similarity

In the present context, geometric similarity is the requirement that the length scales be sufficiently large for long-range dynamical interactions to develop. These length scales are identified from the scales of volcanic edifices and their products. For vertical transport the ratio of the conduit length to its diameter is the key scale. The distance from the volcanic vent to the volatile exsolution level typically ranges from 500 to 5000 m, and observed conduit diameters are in the range 10 to 100 m. This yields a conduit length to diameter ratio of the order of 50. In comparison, this ratio for the experimental tube is 40. *Massol and Jaupart* [1999] suggest that steady state conditions are achieved if the eruption duration is longer than the time required for a fluid packet to ascend from the magma chamber to the surface. In our laboratory setup this timescale is 0.1 s or less, compared with an experimental flow duration of 1 to 2 s. We

therefore consider that our experiments achieve some measure of steady state behavior.

For horizontal transport processes within the conduit the ratio of bubble diameter to conduit diameter is the key scale. The diameter of the experimental conduit is about 10³ times smaller than that of a natural volcanic conduit. Bubble sizes within the solid gum rosin foam fragments recovered from the vacuum chamber range from ~ 1 μm to 1 mm and are similar in appearance to those shown by *Phillips et al.* [1995]. Bubble sizes in natural pumice range from micrometers to centimeters. Most importantly, bubble sizes within the bubbly liquids and foams are much smaller than the conduit diameter in both cases, implying that the effect of bubbles on the fluid rheology [*Manga et al.*, 1998] prior to fragmentation will be similar. In particular, the bubbles are sufficiently small that their buoyant rise velocity is small compared to typical flow velocities; thus the condition of "equilibrium slip" [*Tong and Tang*, 1997; *Melnik*, 2000] is satisfied in both cases. In the experiments demonstrating fragmentation (Plate 1), individual foam slugs and gas pockets sometimes occupy the tube diameter. Gas pockets and magmatic foam slugs can also occupy the entire conduit width in smaller-scale volcanic eruptions [*Vergnolle et al.*, 1996].

Our experiments were conducted in a smooth, effectively rigid-walled (maximum strain 10⁻⁵) glass tube. Hence mechanisms for the generation of pressure oscillations that rely on the elastic deformation of the conduit walls [*Julian*, 1994] or changes in conduit cross section [*Morrissey and Chouet*, 1997b] cannot be investigated. The tube walls are impermeable; therefore our experiments do not simulate the effects of either forced injection of groundwater into the conduit or loss of volatile species through the conduit wall, both of which may occur in volcanic systems and have implications for flow behavior [*Eichelberger et al.*, 1986; *Jaupart*, 1998]. Consequently, all experimental observations of pressure oscillations and flow regimes in the expanding bubbly flows presented here are interpreted in terms of fundamental processes of bubble growth and bursting or flow expansion.

2.2. Thermodynamic Similarity

Volume expansion in the experimental and natural systems depends on the number of molecules of volatile species exsolved as gas to drive the flow and on the ratio of initial to final pressures (decompression ratio), both of which are related through the volatile solubility law. The speciation and diffusivity of the volatiles will determine the rates at which the exsolution process can proceed. These rates are demonstrably high enough in both natural and experimental systems to generate flow fragmentation. We use units of moles per cubic meter for volatile concentration so that unit volumes of both volatile-saturated magma and gum rosin will expand by similar amounts when the ratio of initial to final pressures remains similar. The solution concentrations used in our experiments (15-30 wt % organic solvent in gum rosin, see Table 1) are therefore equivalent to 2-4 wt % water in magma provided the decompression ratios are similar.

The averaged pressure gradient for explosive volcanic flow between exsolution level and vent is $\approx 5 \times 10^7 / 2000 = 25$ kPa m⁻¹ [*Massol and Jaupart*, 1999]. The measured tube base pressure for our experiments is ≈ 20 kPa for ether-driven flows, yielding an average pressure gradient of ~ 13 kPa m⁻¹. Given that the experimental liquid density (≈ 1000 kg m⁻³) is half that of magma (≈ 2000 kg m⁻³), the contribution of the streamwise pressure gradient to flow velocity and acceleration should be similar at laboratory and volcanic scales. The ratio of initial (exsolution level) to final (vent) pressure, which indicates the degree to

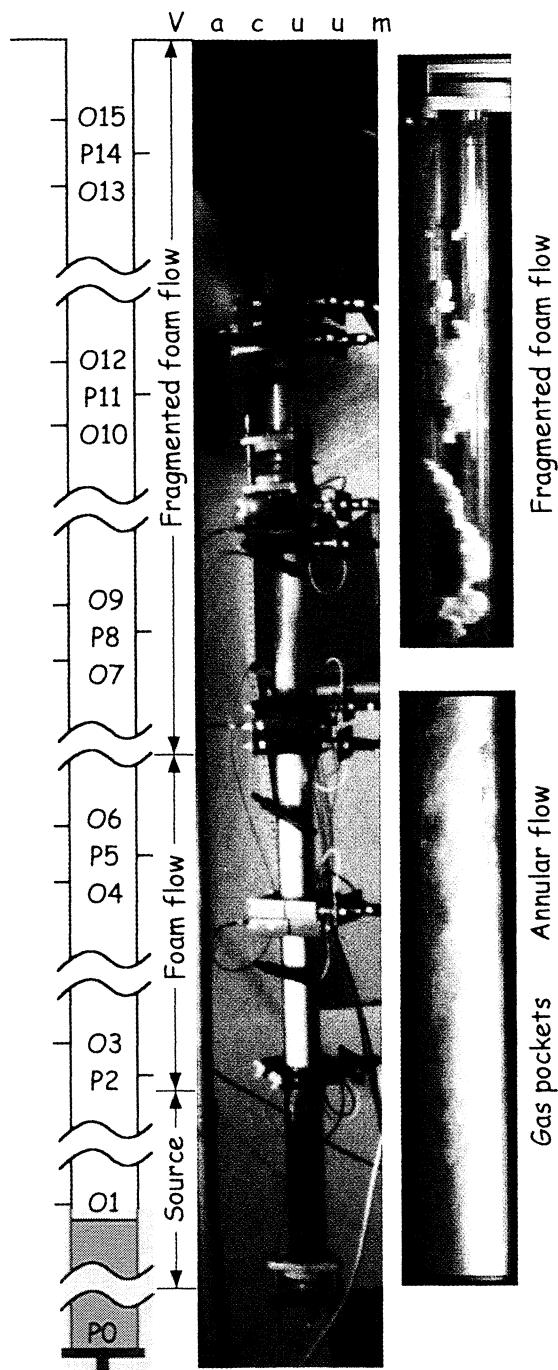


Plate 1. Schematic diagram of experimental system. Optical (O) and pressure (P) transducers are marked. The tube is isolated from the vacuum chamber with a thin plastic rupture disk. A still film camera image shows a fragmenting diethyl ether-driven foam flow in progress, illustrating the growth of foam from the liquid interface and the unfragmented and fragmented regions of the flow. Digital video frames (1/4000 s) show "typical" fragmented, gas-at-wall annular, and gas-pocket-at-wall regions of the flow.

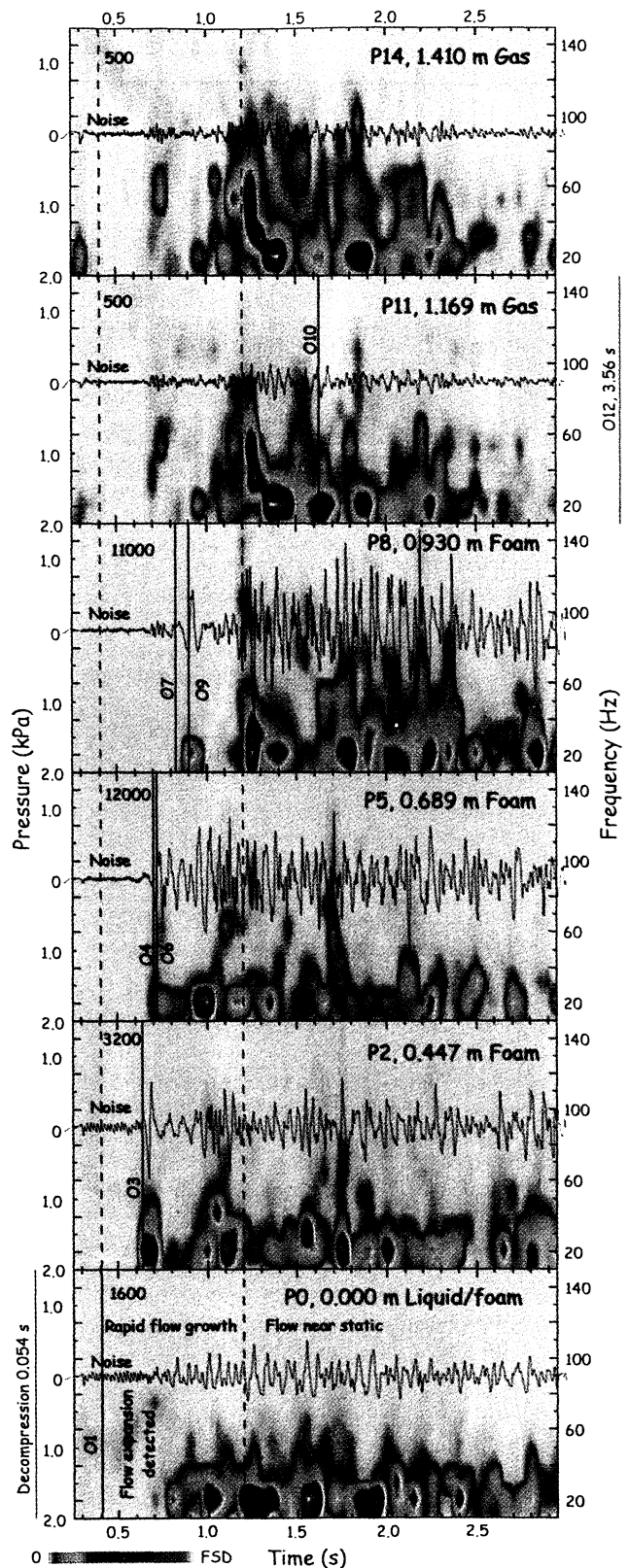


Plate 2. Band-passed pressure data (10-150 Hz) and spectrograms obtained during the nonfragmenting acetone-driven flow. Spectrogram full-scale deflection (FSD) is given in the top left corner of each panel and can be compared to the amplitude of the band-passed pressure signal for each P transducer. Vertical lines represent the times of optical detection of the foam flow at the optical transducers adjacent to each pressure sensor. The time of tube decompression and detection of foam at O12 are beyond the limit of the plots. The noise signal can be seen in the first 0.6 s of each transducer data.

Table 1. Solution and Experimental Conditions Used^a

Run	Volatile, wt %	Volume, ml	Viscosity, Pa s	Vacuum, Pa	P_{svp}/P_v
1	21.8±0.2 acetone	274±1	1.07±0.05	5000	4
2	22.4±0.2 acetone	315±1	0.24±0.05	<10	>2000
3	19.0±0.2 ether	273±1	1.93±0.05	<10	>6000

^a P_{svp} is the solvent vapor pressure and P_v is the vacuum chamber pressure.

which a system can expand, ranges from 1 to 5000 in our experiments, encompassing the range 10 to 1000 for magmas.

Magma and gum rosin both display strong volatile-content-dependent viscosities. Figure 1 shows the viscosity plotted as a function of volatile content for gum rosin with acetone [Phillips *et al.*, 1995] and ether (this study), together with the empirical curve for hydrated rhyolite determined by Hess and Dingwell [1996]. The viscosity of the experimental fluids displays changes with volatile content that are similar to the data of Hess and Dingwell [1996], although the increase in viscosity with volatile degassing is more pronounced in the experimental solutions, which show a viscosity increase of some 12 orders of magnitude for complete degassing compared to a factor of 10^6 for rhyolite. This is likely to enhance any physical phenomena dependent on changes in liquid viscosity occurring during degassing and to enable such phenomena to occur over smaller, i.e., experimental, length scales.

Brittle failure of silicate glass, when subjected to sufficiently high strain rates, is a postulated mechanism of magma fragmentation during explosive eruptions [Dingwell, 1996]. Papale [1999] uses the Maxwell relation as a fragmentation criterion. This relation is stated as $dv_z/dz > k/\tau = kG_\infty/\mu$, where dv_z/dz is the elongational strain rate, k is a constant, G_∞ is the elastic modulus at infinite frequency, and μ is the zero-frequency viscosity. For a wide range of natural compositions, $k = 0.01$ and G_∞ is in the range 3-30 GPa [Dingwell and Webb, 1989]. Using a sound speed of 2000 m s^{-1} measured in gum rosin-organic solvent solutions and a density of 1000 kg m^{-3} , we estimate G_∞ to be $\approx 4 \text{ GPa}$. The value of k is not known, but we suggest above that strain rates are similar. The viscosity of gum rosin-organic solvent solutions is generally lower than that of hydrated rhyolite, but increases more rapidly as degassing proceeds (Figure 1). Therefore both the natural and experimental fluids may experience the transition from viscous fluid to brittle solid behavior as the viscosity increases during degassing.

2.3. Dynamic Similarity

Dynamic similarity is the requirement that natural and experimental systems exhibit the same flow regimes. This means not only matching the flow Reynolds number (Re) but also conditions of bubble deformation and acoustic velocity, as we are also interested in the transmission of pressure fluctuations. We require the quantification of suitable nondimensional parameters and a demonstration that their values fall within the ranges defining different flow regimes. Quoting Mayinger [1981] as cited by Tong and Tang [1997, p. 355] "Scaling by use of dimensionless numbers only is limited in two-phase flow to simple and isolated problems, where the physical phenomenon is a unique function of a few parameters." Similarity parameters for viscous two-phase flows are not yet well-established [Tong and Tang, 1997; Kaminski and Jaupart, 1998], so here we are limited to a discussion of matching appropriate length scales in the thermodynamic and dynamic behaviors.

The Reynolds number is defined as the ratio of inertial to viscous forces within the expanding flow and may be expressed as $Re = (U \rho r)/\mu_e$, where r is the conduit radius, μ_e is the effective viscosity of the bubbly liquid, ρ is the fluid density, and U is the horizontally averaged velocity. Using data from Massol and Jaupart [1999], we can estimate Re at and just above the exsolution level, where gas-volume fractions are small and strain rates low. For a gas-volume fraction $\phi \leq 0.45$ and capillary number (see below) $Ca = 0.3$ (near spherical bubbles) the fluid viscosity is <25% greater than the liquid viscosity [Manga *et al.*, 1998], i.e., not a significant effect for the purposes of this estimate. Using values of $U = 1 \text{ m s}^{-1}$, $\rho = 2000 \text{ kg m}^{-3}$, $r = 50 \text{ m}$, and $\mu_e = 10^6 \text{ Pa s}$ yields $Re \approx 0.1$ for a rhyolitic eruption. For gum rosin solutions with $U = 1 \text{ m s}^{-1}$, $\rho = 900 \text{ kg m}^{-3}$, $r = 0.02 \text{ m}$, and $\mu_e = 10 \text{ Pa s}$ we obtain $Re \approx 2$. In both cases, the initial flow expansion takes place in a laminar flow regime ($Re < 2000$) and may remain in this regime until the onset of fragmentation [Massol and Jaupart, 1999] because of the rapid nonlinear increase in liquid viscosity during degassing in both natural and experimental liquids (Figure 1). Detailed consideration of the flow body forces acting in a fully-developed foam flow is beyond the scope of this discussion (see above), and application to bubbly liquids and foams with a yield strength and complex rheology [Prud'homme and Khan, 1996] and with longitudinal and radial variations of many flow variables over short distances [Massol and Jaupart, 1999] is not clear. However, natural and laboratory flows exhibit rapid increases in velocity (i.e., strain rate), liquid viscosity, and gas-volume fraction (i.e., fluid density decreasing) as degassing proceeds, implying that the physical parameters underlying the Reynolds number are all changing in the same direction in both systems and therefore suggest that both are likely to exhibit a similarly rich range of flow behaviors between the exsolution and fragmentation levels. Above the fragmentation region the flow viscosity becomes that of the gas phase [Massol and Jaupart, 1999], the velocity increases rapidly, and the density decreases, resulting in a very large Re . Flow is then implied to be turbulent in both natural [Jaupart, 1996] and laboratory flows upstream of fragmentation. The Re similarity during the early and late stages of the natural and experimental flows, combined with the similarity in the physical properties of the fluids, implies similar dynamic flow behavior for both systems.

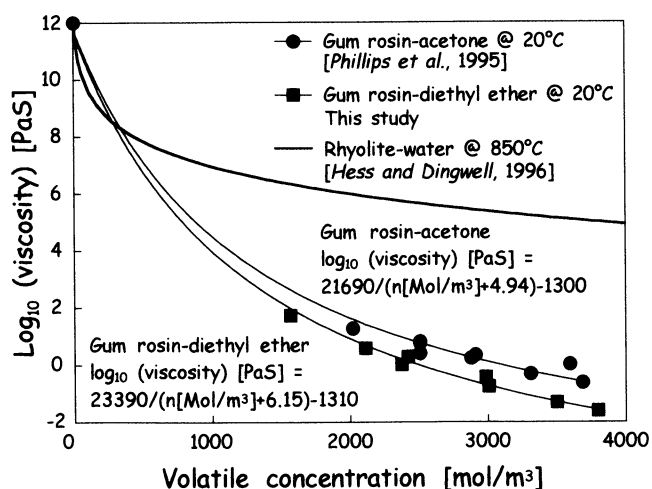


Figure 1. Viscosity versus volatile concentration. The bold solid line shows the data for hydrated rhyolite at 850°C obtained by Hess and Dingwell [1996]. Solid dots are data for gum rosin-acetone at 20°C obtained by Phillips *et al.* [1995]. Solid squares are data for gum rosin-diethyl ether at 20°C .

Massol and Jaupart [1999] suggest using the dimensionless conduit radius to height ratio as a scaling parameter. This is small for both experiments (0.013) and eruptions (≈ 0.02). *Massol and Jaupart* also suggest the use of this ratio multiplied by the Reynolds number (Re). These parameters rely on the relevant scale being the conduit height and therefore assume that radial pressure gradients are negligible. However, because of the strong dependence of magma viscosity on dissolved water contents the flow pressures vary on much smaller length scales when fragmentation occurs [*Massol and Jaupart*, 1999; *Melnik*, 2000]. The strong dependence of gum rosin viscosity on organic solvent contents in the experimental fluid implies that the conduit length is not an appropriate experimental length scale either and that radial pressure gradients are likely to be present both in volcanic and experimental conduits. Indeed, the more rapid increase of viscosity with degassing in the experimental fluid (Figure 1) implies that this phenomenon will be stronger in the experiments. Therefore use of a fluid system with a strongly volatile-dependent viscosity, as considered here, is likely to be an essential prerequisite for laboratory simulation of explosively degassing magma flows within volcanic conduits.

The fluid rheology is complicated by the presence of bubbles [*Manga et al.*, 1998] that have a variable number per unit volume and variable size and can deform during fluid flow. The presence of bubbles can increase or decrease the apparent viscosity and produce highly non-Newtonian and strain-history-dependent rheology at high gas-volume fractions. A dimensionless parameter for the behavior of bubbles in viscous flows [*Manga et al.*, 1998] is the capillary number, $Ca = (d\epsilon/dt)\mu r/\sigma$, in which ϵ is the strain, σ is the surface tension, μ is the liquid viscosity, and r is the bubble radius. Ca represents the ratio of the bubble deforming to bubble restoring forces. At low Ca (bubbles closely spherical), the bubbly fluid or foam viscosity is generally greater than that of the liquid phase, while at high Ca (bubbles highly elongated) the bubbly fluid or foam viscosity is generally less than that of the liquid phase [*Manga et al.*, 1998]. The existence of tube pumice [*Marti et al.*, 1999] suggests that $Ca \gg 1$ for explosive volcanic flows. Microscope observation of fractured surfaces on foam fragments generated during high decompression ratio experiments often shows elongated bubbles, as illustrated by *Phillips et al.*, [1995]. This implies that $Ca \gg 1$ for the fragmenting flows. Unfortunately, the highly friable nature of the opaque gum rosin foam makes detailed study of the bubble shapes and sizes difficult. Overlap of capillary number and gas-volume fraction (see below) implies that the presence of bubbles will have similar rheological effects [*Manga et al.*, 1998] in both the natural and experimental fluids.

We are specifically interested in the pressure oscillation behavior of the experimental system; therefore the acoustic velocity of the experimental fluid as a function of gas-volume fraction should behave in a similar fashion to that in magmatic systems. Calculations indicate that the acoustic velocity of magmatic fluids decreases rapidly from that of the single phase liquid to a minimum between 100 and 200 m s^{-1} at a gas-volume fraction ≈ 0.8 , then rises again to the velocity of the single gas phase. Gas-volume fractions in pumice generally range from 0.6 to 0.8. Gum rosin organic solvent fluids display the same behavior, but the lower liquid density, bulk modulus, and system pressure yield an acoustic velocity minimum of 10 to 15 m s^{-1} at a gas-volume fraction of 0.5. The gas-volume fractions of preserved experimental foams range from 0.75 to 0.9. We can therefore expect strong similarity between the resonance behaviors of the natural and experimental fluids.

The ratio of flow velocity to acoustic velocity is known as the Mach number. Theoretical simulations suggest that volcanic conduit flows are often close to Mach 1, and choked, at the vent

[*Sparks et al.*, 1997; *Morrissey and Chouet*, 1997b]. The ratio of the measured velocities of foam fragments near the tube top in the experimental system to the calculated acoustic velocities at appropriate gas-volume fractions yields Mach numbers in excess of 0.8. The near constant maximum flow velocity associated with a three time increase in driving pressure between acetone- and ether-driven flows suggests that the vent Mach number is approaching unity. This implies that there is a degree of similarity in the Mach numbers of the flows in a volcanic conduit during explosive activity and the Mach numbers of the flows in the experimental tube at high supersaturations.

We are observing pressure oscillations within the experimental fluids and comparing these to estimates of pressure fluctuations generating volcano-seismic signals; therefore we require a means of comparing oscillation amplitudes in systems with greatly differing absolute pressures. Acoustic resonance in boiling water flows may have amplitudes representing a significant fraction of the pressure level [*Tong and Tang*, 1997]. Therefore we adopt the ratio of oscillation amplitude to average pressure ($\Delta P/P$) as a means of comparison between different systems.

3. Methods

A 1.5-m-long (3.8 cm internal diameter) tube of borosilicate glass is vertically mounted beneath a vacuum chamber of 0.4 m^3 volume (Plate 1). The experimental tube, at atmospheric pressure, is isolated from the vacuum chamber by a plastic membrane with an imbedded hot wire rupture system. Rupture of the membrane initiates the experiment. Pressure transducers (P) with a frequency response of 10 Hz to 100 kHz are combined with optical transducers (O) to provide measurements of the flow (Plate 1). The transducers are logged with a sampling frequency of 40 kHz using a 12-bit data acquisition board mounted in a PC.

Gum rosin powder is mixed with either acetone or diethyl ether to manufacture the experimental source liquid [*Phillips et al.*, 1995]. The initial viscosities (Table 1) of the solutions are measured using a falling ball viscometer. The solution volatile content (Table 1) is measured by fully degassing samples of the experimental liquid at 80°C overnight and cooling to give solid gum rosin, then measuring the resultant weight loss.

The O sensor data are used to monitor both the presence of gas (low attenuation) and foam (high attenuation) in the tube at each sensor position and to provide a visual indication of where foam slugs and gas pockets are positioned in the tube at any one time. The P transducer data are exported to the Seismic Analysis Code (SAC) program (available at <http://www-ep.es.llnl.gov/www-ep/esd/seismic/sac.html>) for scaling, frequency band-passing, and spectral analysis. To explore the range of signal amplitudes and frequencies, data were band-passed, and spectrograms were generated for 10-150 Hz, 50-500 Hz, 500-1000 Hz, and 1-5 kHz frequency ranges. Blank runs and experimental baseline data were analyzed for transducer noise, apparatus oscillations, and other artifacts. Data presented here are considered artifact free and above noise unless otherwise stated.

4. Results and Interpretation

Table 1 lists the conditions for the three experiments we document here. These experiments cover a range of source liquid supersaturation resulting from decompression. We limit ourselves to documenting the major observations with sufficient text to guide the reader through the figures.

4.1. Low Supersaturation Flow

The experimental oscillation frequencies are consistent with longitudinal and radial resonance of the foam column and occur

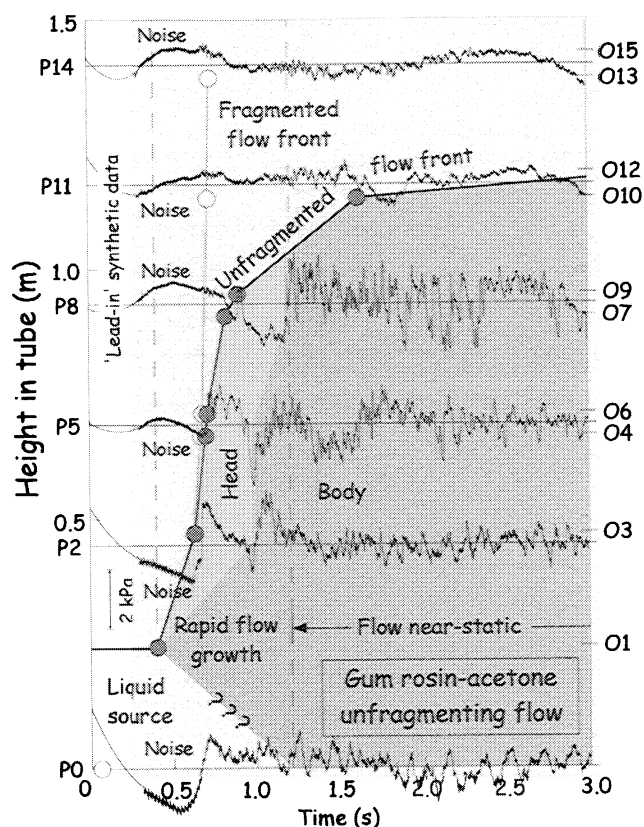


Figure 2. Height versus time plot of optical and pressure sensor data for unfragmenting acetone-driven flow. The positions of the optical (O) and pressure (P) transducers are indicated. Open symbols represent the times at which the first foam fragments are detected (five detected on initial decompression) and solid symbols mark the unfragmented flow front detected by the optical sensors. The symbol at zero height represents the time at which P14 detected pressure falling below 99 kPa on decompression. Data are shown for each P transducer at the appropriate tube height. Pressure data are shown after correction to remove transducer drift. The noise-free section of pressure data between 0.1 and 0.3 s is synthetic data included to reduce high-pass filter end effects. The pressure range is indicated by the scale bar. Shading indicates regions of the observed flow regimes (see text for details).

once the resonator length is stable on a time scale of two oscillation cycles. We suggest that similar processes take place in slowly degassing, i.e., effusive and weakly explosive, magmatic flows in conduits.

Decompression to low volatile supersaturations produces essentially unfragmenting foam flows and displays very minor fragmentation upon initial decompression. Figure 2 shows the positions of the fragmented and unfragmented flow fronts, the oscillatory pressure data, and the evolution of different regions of the flow as a function of time for an acetone-driven flow into a chamber pressure of 5 kPa air. Five fragments were detected ahead of the unfragmented flow front. This was typical of the initial behavior of all the low-supersaturation experiments carried out. There is a time delay of 0.35 s between decompression and the detection of flow expansion. This time is presumably required for the generation of critical bubble nuclei. Following bubble nucleation, the flow behavior can be divided into three stages based on the expansion rate. These are (1) rapid flow expansion between 0.4 and 1.2 s, (2) static foam column between 1.2 and

10 s, and (3) collapsing foam after 10 s. We concern ourselves with the first two stages here.

Plate 2 shows spectrograms for each P transducer during the interval 0.35–2.95 s, along with the 10–150 Hz band-passed pressure data. Vertical lines identify the times at which the foam front was detected by the O transducers. As the foam front passes P transducers 2, 5, and 8, there is a rapid pressure rise (Figure 2), which produces the first significant signal on the spectrograms (Plate 2). The pressure rise is highest at P2 and decreases through P5 and P8 (Figure 2). The magnitude of the pressure rise reflects the hydrostatic pressure in the fluid column. The following few tenths of seconds are characterized by low-amplitude oscillations in the 10–30 Hz range. The ratio $\Delta P/P$, in which P denotes the solvent saturated vapor pressure ($\text{svp} \approx 20 \text{ kPa}$ at 20°C for acetone), is $\approx 1\%$ for these oscillations. Following another pressure step near 1 s at P2 and P5 and near 1.2 s at P8 (Figure 2), higher-amplitude pressure oscillations ($\Delta P/P \approx 5\text{--}10\%$) are detected. These show a 20-Hz peak with other discernable peaks in the 80 to 100 Hz range (Plate 2). These two regions with different oscillation signatures suggest different flow behaviors, and are identified in Figure 2 as flow "body" and flow "head."

The foam did not reach P11 or P14 during the course of the analyzed data; therefore oscillations in these regions of the tube occur in the gas phase. P11 and P14 show very similar spectrograms (Plate 2) with oscillations peaked in the 30 to 70 Hz band occurring between 1.18 and 1.25 s. The signal then narrows around a 20-Hz peak after 1.4 s, with weaker contributions from higher frequency oscillations.

Figure 3 shows a schematic interpretation of an unfragmenting flow in the rapid expansion phase, with the position of flow regions as a function of time as indicated in Figure 2. Initial degassing during the rapid expansion stage produces a volatile-poor flow head with detectable pressure oscillations. Beneath the flow head is a more volatile-rich, hence lower-viscosity, flow body sustaining higher-amplitude oscillations. The pressure step separating these two regions (Figure 2) exceeds hydrostatic values and may be associated with increased radial stress [Massol and Jaupart, 1999] in the foam as it flows. Pressure oscillations in the flow body do not propagate into the gas above the flow, implying weak coupling between the gas and oscillating foam. This suggests that the flow head has different acoustic properties than the flow body. The flow head thus appears to act as an acoustic reflector or absorber.

Transducer P0 detected continuous oscillations only after 0.7 s (Figure 2 and Plate 2). This implies some form of acoustic discontinuity between the oscillating flow body and the source liquid between 0.4 and 0.7 s. Images (e.g., Plate 1) show that the expanding foam originates from the surface of the gum rosin-organic solvent solution. The interface between liquid and foam presents a strong velocity discontinuity of $\approx 2000 \text{ m s}^{-1}$ on the basis of our measured acoustic velocity of 1950 m s^{-1} in the source liquid and calculated foam velocity of 10 m s^{-1} . Benoit and McNutt [1997] propose that such a velocity-controlled boundary forms the base of the resonating conduit at Arenal Volcano. They also invoke a velocity-controlled boundary at the top of the conduit, formed here by the flow head. This demonstrates the experimental generation of acoustic structures similar to those proposed to explain field data from volcanic conduits.

The stable nature of the oscillation frequencies is suggestive of a resonant oscillation. The establishment of a near-stable resonator length over a period of at least two oscillation cycles (0.1 s at 20 Hz) may be a factor contributing to the increase in oscillation amplitude as the flow wanes at $\approx 1 \text{ s}$ (Figure 2). The length of this resonator (the flow body) is estimated to be 0.5 m at 1 s, assuming that the flow head boundary is located between P2 and P5 and that some source liquid remains. This suggests an acoustic velocity of 20 m s^{-1} at the fundamental frequency of 20

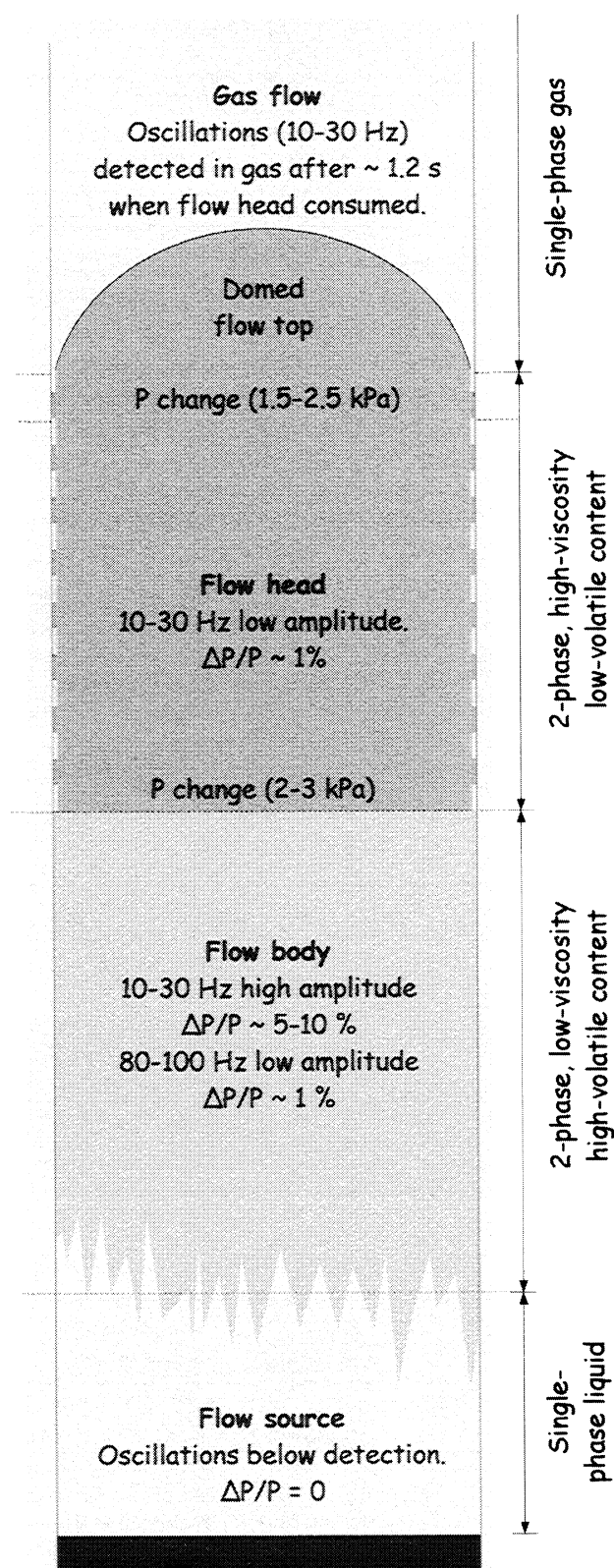


Figure 3. Schematic representation of flow regimes and pressure oscillations during the rapid expansion phase of the acetone-driven unfragmenting foam flow.

Hz. Assuming that most of the degassed acetone is locked within the bubbles, we obtain an average gas-volume fraction of 0.75-0.80. The calculated value of acoustic velocity under nonequilibrium conditions [Kieffer, 1977] is $\approx 12 \text{ m s}^{-1}$ for this gas

fraction. This may imply that 20 Hz is not the fundamental frequency but the first harmonic. As the frequency response of both the P transducers and the spectral analysis method is poor below $\approx 10 \text{ Hz}$ we may be observing the fundamental oscillation frequency but be unable to resolve it from the first harmonic. The need for resonator stability may explain the sudden onset of seismic and acoustic resonant oscillation from broadband signals observed at Arenal Volcano. This may also provide an explanation for the intervals of seismic and acoustic quiescences that appear to follow increasing rates of acoustic and seismic frequency changes [Garcés *et al.*, 1998]. According to our observations, such quiescences may be indicative of an increasing rate of change of acoustic velocity and/or cavity dimension leading to resonator instability.

With the removal of the flow head by redissolution of acetone vapor degassing from the flow body, as evidenced by the onset of acoustic oscillation at 1.2 s, we may expect a frequency reduction as the length of the oscillating foam column increases. At 1.2 s the total foam column is only $\approx 5 \text{ cm}$ longer than at 1 s; however, the oscillating flow body length has increased from ≈ 0.5 to 1.03 m (Figure 2). This yields a fundamental resonant frequency near 6 Hz and a first harmonic near 12 Hz. This shift is not apparent in the Plate 2 spectrogram, probably because these frequencies are at the limit of the sensor detection capabilities as stated above. Visual analyses of the pressure traces (Figure 2) from P0 between 1.2 and 1.6 s and after 1.8 s provide evidence of two to three cycles of oscillations with peak-to-peak amplitudes of 1 kPa at frequencies $< 10 \text{ Hz}$. These oscillations are also present in the P5 and P8 data after 1.8 s (Figure 2). These may represent the fundamental longitudinal oscillation frequency. The weak spectral peaks ($\Delta P/P \approx 1\%$) at 80-100 Hz (Plate 2) yield a dimension of $\approx 0.055 \text{ m}$ for the fundamental frequency, assuming an acoustic velocity of 10 m s^{-1} . This is close to the radial dimension of the flow tube and may represent a radial resonance mode.

Transducers P11 and P14 detect oscillations after $\approx 1.2 \text{ s}$. Figure 2 shows that flow expansion is small and decreasing by this time, and we chose this time as the start of the static foam column phase. This choice is supported by the presence of strong oscillations at P0 after 1.2 s, which point to the removal of the basal velocity discontinuity and exhaustion of the source liquid. The onset of oscillations in the gas implies a removal of the top acoustic discontinuity. Pressure oscillations can then propagate into the gas above the flow. The foam column is now degassing by bubbles coalescing and bursting at the flow front rather than by foam growth [Phillips *et al.*, 1995]. An approximate timescale for bubble coalescence is given by the expression $t = 2r\eta/\sigma$ [Jaupart and Vergnolle, 1989], where r is the bubble radius, η is the viscosity, and σ is the surface tension. Using values of 20 μm , 100 Pa s, and 0.029 N m^{-1} [Phillips *et al.*, 1995], respectively, suggests a coalescence timescale of $\approx 0.1 \text{ s}$, implying that significant bubble coalescence can occur on the $> 1 \text{ s}$ timescale of the experiment.

This experiment shows that acoustic pressure oscillations are a fundamental consequence of foam expansion and collapse and probably result from dynamic instability [Tong and Tang, 1997]. The oscillations do not require changes in tube cross section, transonic speeds, or other special conditions to occur. It is known that energetic noise emissions in bubbly liquids originate in the collective oscillation of those bubbles [Lu *et al.*, 1990], but the fundamental causes of pressure fluctuations stimulating the resonance are not clear. However, the nonlinear behavior of viscosity, and hence diffusivity, as a function of volatile content in a nonequilibrium compressible system may play a role. We suggest that a possible oscillation generation mechanism during foam stasis and collapse is due to bubble coalescence and

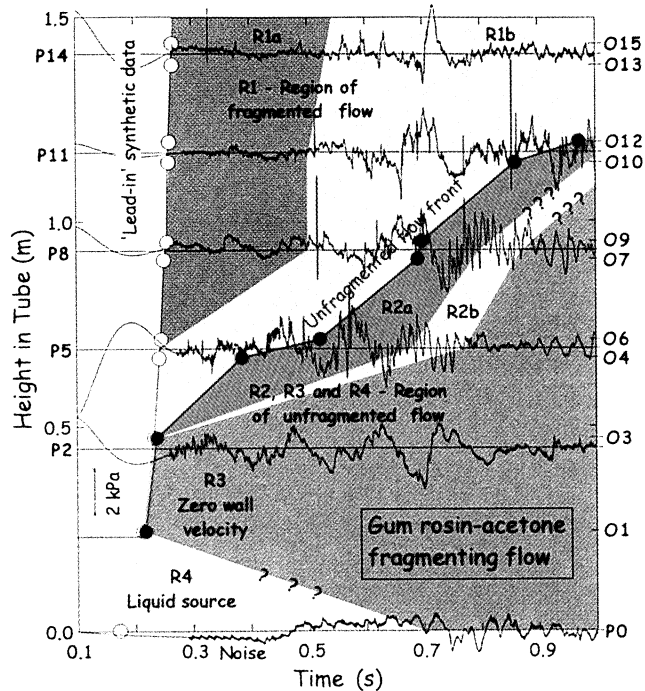


Plate 3. Height versus time plot of optical and pressure sensor data for the fragmenting acetone-driven flow. The positions of the optical (O) and pressure (P) transducers are indicated. Open symbols represent the times at which the first of 150 foam fragments are detected, and solid symbols mark the onset of unfragmented flow. The symbol at zero height represents the time at which P14 detected pressure falling below 99 kPa on decompression. Pressure data are shown after correction to remove transducer drift. The noise-free section of pressure data between 0.1 and 0.3 s is synthetic data included to reduce high-pass filter end effects. The pressure range is indicated by the scale bar. Shading indicates regions of the observed flow regimes (see text for details).

bursting, a mechanism proposed for the generation of volcanic tremor by Ripepe and Gordeev [1999].

4.2. High Supersaturation Flow

These experimental flows include a number of flow regions with characteristic pressure oscillation behaviors. We suggest that such behaviors may be observed in strongly explosive magmatic flows in conduits.

The general behaviors of acetone- and ether-driven flows are illustrated in Plates 3 and 4, and the flow parameters are listed in Table 1. The transition between fragmented and unfragmented acetone-driven flow moved up the tube with an average velocity of 1 m s^{-1} , thus defining the field in time and space within which the flow was fragmented (Plate 3). The flow rapidly waned as the source solution became depleted in $\approx 1 \text{ s}$. Fragmentation effectively ceased at this point, and the unfragmenting foam flow slowly expanded up the tube with occasional emission of slowly moving foam slugs from its top surface. The fragmented ether-driven flow front (Plate 4) reached a peak velocity of 34 m s^{-1} , similar to that of the acetone-driven flow (32 m s^{-1} , Plate 3) despite having potentially 3 times the driving pressure. This implies that these flows were overpressured in a manner similar to some explosive volcanic conduit flows [Sparks *et al.*, 1997]. The ether-driven flows behaved differently from the acetone-driven flows, in that the detected fragmentation level was much

more positionally stable (Plate 4). The fragmentation level was observed to oscillate around P8 for $\approx 1.4 \text{ s}$. Fragmentation activity then rapidly decreased with occasional fragments spalling from the flow front. The unfragmented foam flow then slowly ascended the tube, emerging into the vacuum chamber some time after logging ceased. The correlation between pressure oscillation behavior and flow regime is apparent to the eye in Plates 3 and 4, and we now consider further the data from transducers P2 and P8 for acetone- and ether-driven flows.

Single cycle oscillations are detected by transducer P2 (Plate 5) between 0.45 and 0.75 s during the acetone-driven flow. Multicycle oscillations with strong LP character reoccur between 1.05 and 1.35 s. These oscillations occur in a narrow band of 10–30 Hz and have peak-to-peak amplitudes of 1 kPa ($\Delta P/P \approx 5\%$). There is also some indication of oscillations in the 80–100 Hz range. The onset of these oscillations corresponds to the decline

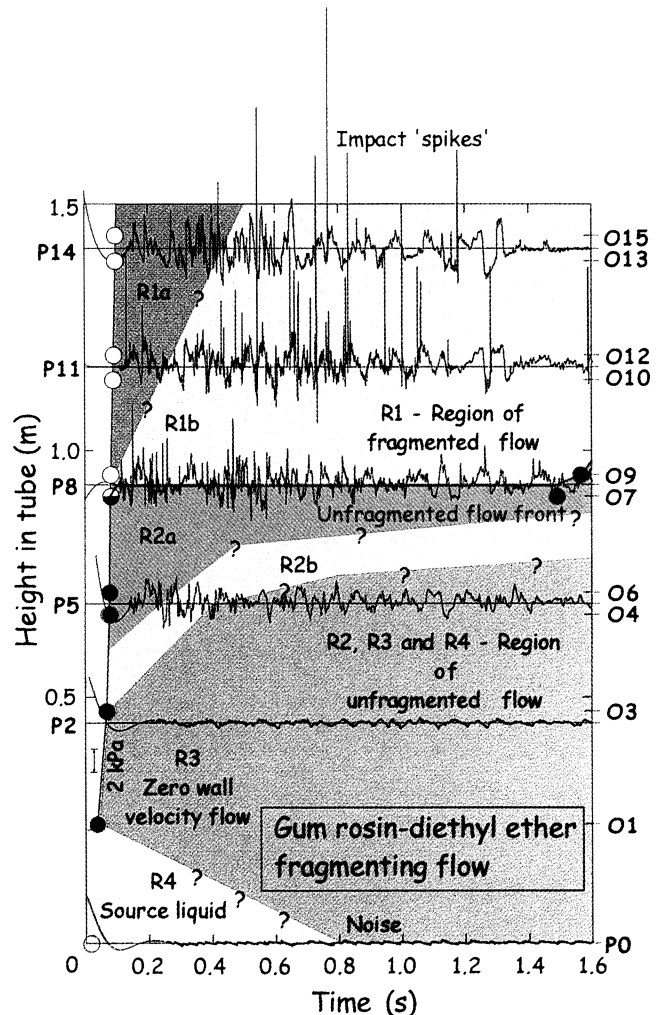


Plate 4. Height versus time plot of optical and pressure sensor data for fragmenting ether-driven flow. The positions of the optical (O) and pressure (P) transducers are indicated. Open symbols represent the times at which the first of 270 foam fragments are detected, and solid symbols mark the onset of unfragmented flow. The symbol at zero height represents the time at which P14 detected pressure falling below 99 kPa on decompression. Pressure data are shown after being corrected to remove transducer drift. The noise-free section of pressure data between 0.1 and 0.3 s is synthetic data included to reduce high-pass filter end effects. The pressure range is indicated by the scale bar. Shading indicates regions of the observed flow regimes (see text for details).

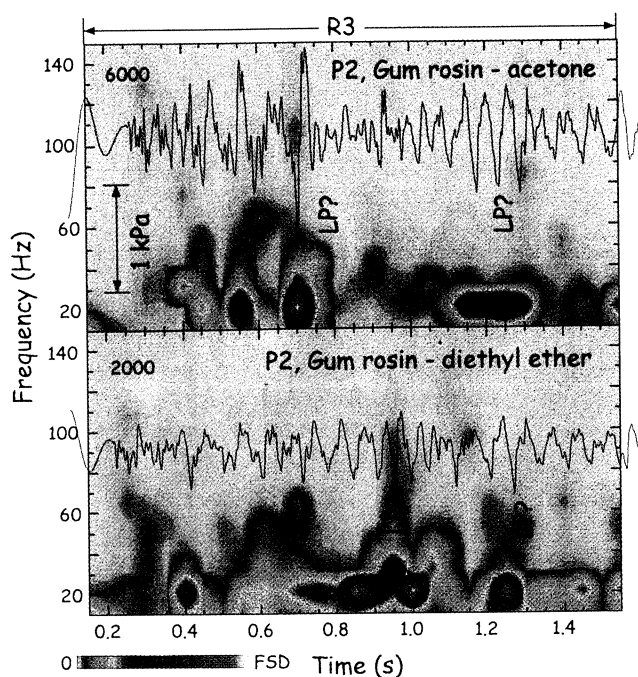


Plate 5. Spectrograms of 10-150 Hz and band-passed pressure data from transducer P2 for acetone- and ether-driven flows. P2 measures data from the zero-velocity-at-wall region (R3) of these flows, which is dominated by oscillations peaking at 20 Hz or less. We indicate where these oscillations are similar to long-period seismic events.

of the flow and establishment of a stable, slow moving foam column. This is similar to the situation observed in the unfragmenting flow. Narrowband oscillations continue after 1.35 s but at reduced amplitudes. The ether-driven flow produces a more continuous signal in the 10-30 Hz range, also including some 80-100 Hz peaks (Plate 5). The peak amplitude of the

signal is a factor of 3 less than, and the average signal amplitude is similar to that in the acetone-driven flow (Fig. 8), that is, $\Delta P/P \approx 3-10$ times less for the ether-driven flow compared with the acetone-driven flow in this region. These observations are consistent with the more stable fragmentation level and indicate that the ether-driven flow is steadier than the acetone-driven flow. This suggests that seismic activity may be stronger and more variable during changes in flow behavior in a volcanic conduit than during a more established flow pattern.

Plate 6 shows optical, pressure, and bandpassed pressure data for transducer P8 during the acetone-driven flow. Regions with different optical and pressure oscillation signatures can be delineated. Region 1 (R1) spans 0.25 to 0.72 s (Plate 3) and corresponds to fragmented flow as detected by the optical transducers O7 and O9 (Plate 6). R1 can be subdivided into R1a and R1b based on the characteristic pressure oscillation behavior as summarized in Table 2. Region 2 (R2) covers 0.72-0.87 s, and can again be subdivided according to the pressure oscillation behavior (see Table 2). Region 3 (R3) moves by P8 after 0.87 s. Table 2 summarizes the oscillation behavior observed in this region. The pressure gradient is higher in R2, especially in R2a, compared to R1 or R3, as indicated by the raw pressure trace (Plate 6), but we are not able to accurately quantify the pressure gradient with the data presented here.

Plate 7 shows optical, pressure, and bandpassed pressure data for transducer P8 during the ether-driven flow. Plate 4 shows that P8 was close to the fragmentation level for most of the flow duration. On the basis of the optical and pressure oscillation signatures (Table 2) the boundary between regions R2a and R1b is seen to pass back and forth past P8 (Plate 7) as the level of fragmentation also oscillates.

Plate 8 gives a schematic representation of the flow regions in the two fragmenting flows described above, and Table 2 summarizes the oscillatory behavior of both flows.

Region 4 contains the source liquid. As in the weakly supersaturated flows, this region remains acoustically isolated from the foam expanding from the liquid upper surface so that pressure oscillations are not significant in R4 (Figure 2, Plates 3 and 4, and Table 2). This implies that pressure oscillations are not

Table 2. Flow Regime Distinction Based on Optical, Pressure and Image Data^a

Flow Region	Optical Transducer	Pressure Transducer	Image Data
1a Fragmented	tube diameter scale gas pockets	low levels of oscillation	foam fragments and gas
1b Fragmented	tube diameter scale gas pockets	significant continuous 0.5-5 kHz signals; wave packets of few kilopascal amplitudes	flow of foam slugs and gas
2a Detached, foam in gas annular	bubbles smaller than tube diameter	as 1b with large amplitude (few kilopascals) broadband oscillations in 10-500 Hz range centered at 80-100 Hz; 10-30 Hz oscillations in ether-driven flow	annular foam-in- gas flow
2b Detached, gas pocket at wall	bubbles smaller than tube diameter	narrowband signal centered at 80-100 Hz; 10-30 Hz oscillations in ether-driven flow; low amplitude 0.5-5 kHz signals with no wave packets	gas-pocket-at- wall flow
3 Zero wall velocity	bubbles smaller than tube diameter	10-30 Hz signal of a few kilopascals amplitude; low amplitude 80-100 Hz signal occasionally detected	foam flow wets tube wall
4 Static liquid		no oscillations detected	foam grows from liquid surface

^aSee also Plate 8.

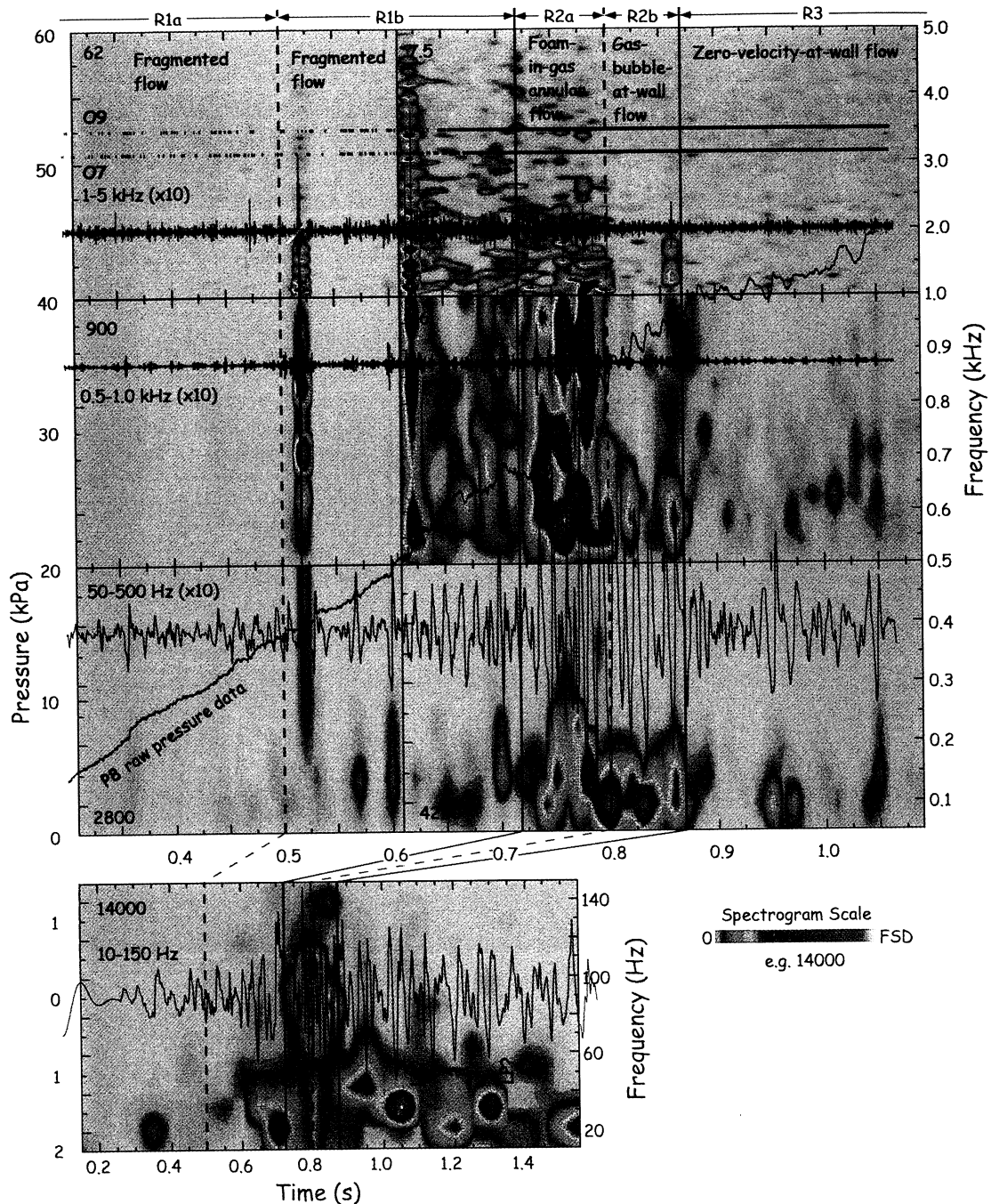


Plate 6. Data from P8 during fragmenting gum rosin-acetone foam flow. Diagonal trace indicates raw data from P8. Traces offset to 15, 35, and 45 kPa are 50-500 Hz, 0.5-1.0 kHz, and 1-5 kHz band passed data displayed at 10X actual amplitude. Two top lines represent the presence of foam at O7 and O9. Background spectrograms show frequencies in the range 50-5000 Hz with each of the six panels (demarked by scaled axes) having the full-scale deflection (FSD) as shown at the top left, or bottom left, corners. Flow regions and their subregions are identified at the top. The band-passed data and spectrogram in the 10-150 Hz band are shown in bottom with a different timescale.

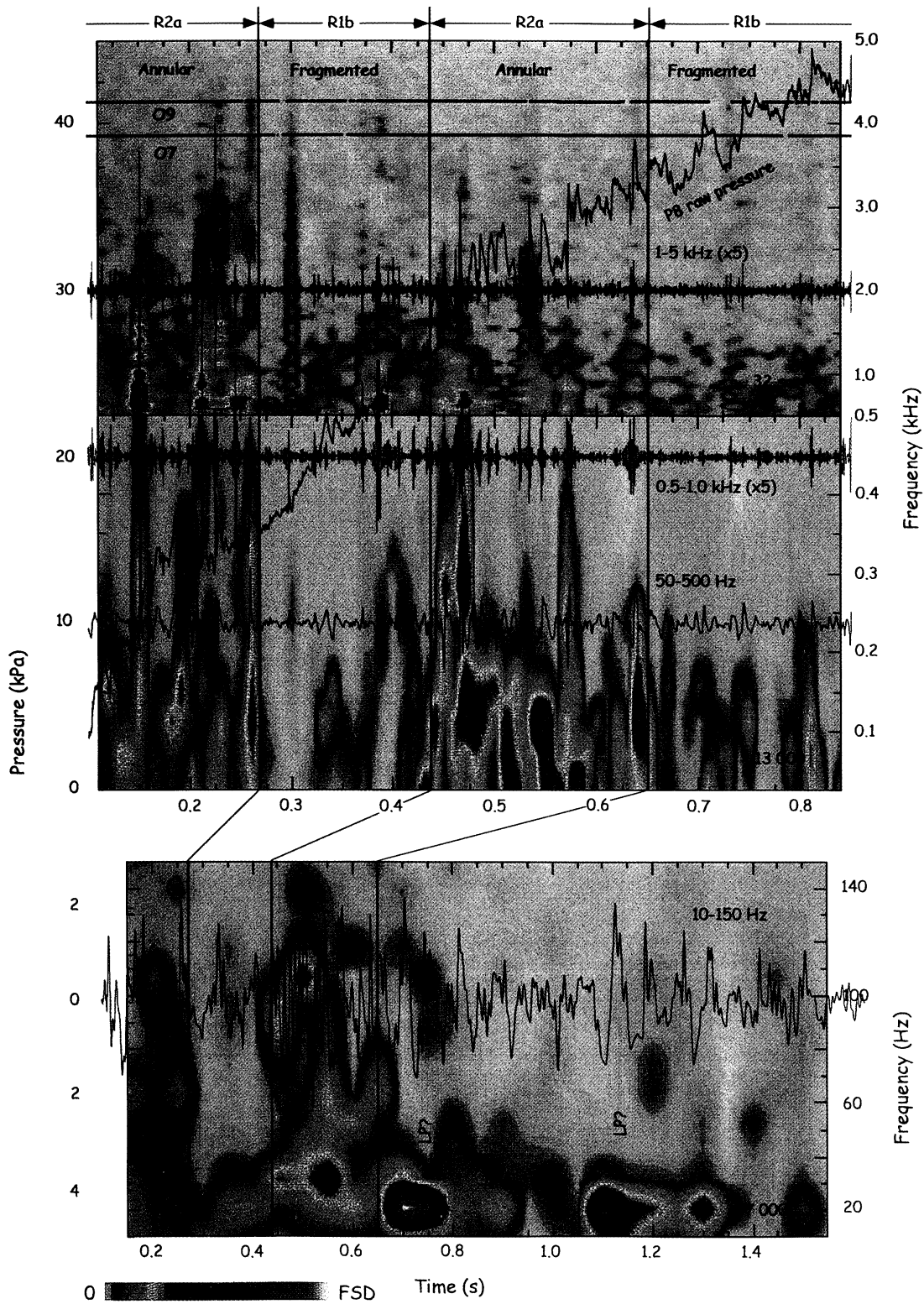


Plate 7. Data from P8 during fragmenting ether-driven foam flow. Diagonal trace indicates raw data from P8. Traces offset to 10, 20, and 30 kPa are 50-500 Hz, 0.5-1.0 kHz, and 1-5 kHz band-passed data displayed at 1X, 5X and 5X actual amplitude, respectively. Two top lines represent the presence of foam at O7 and O9. Background spectrograms show frequencies in the range 25-5000 Hz with each of the two panels having the full-scale deflection (FSD) as shown at bottom right corners. Sqrt indicates a square root scale. Flow regions and their subregions are identified at the top. The band-passed data and spectrogram in the 10-150 Hz band are shown in bottom panel with a different timescale.

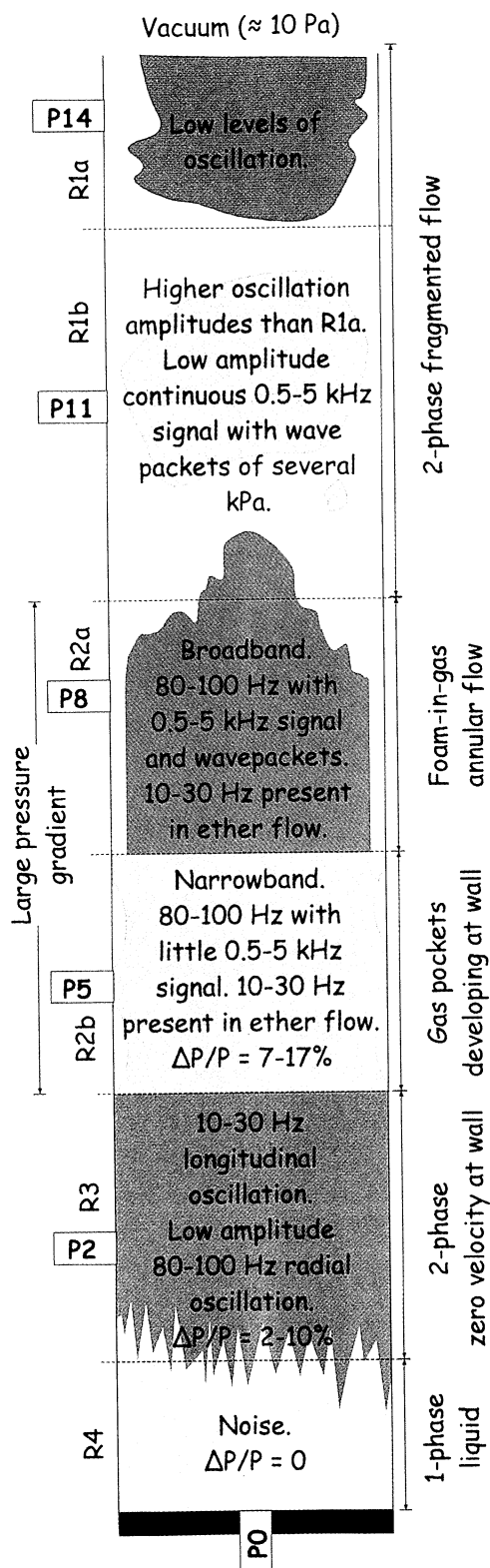


Plate 8. Schematic representation of flow regimes and pressure oscillations in a fragmenting foam flow. The positions of the pressure transducers are indicated, and the flow regions are positioned as in the acetone-driven flow at ~ 0.7 s, and ether-driven flow at ~ 0.3 s.

generated within the source liquid. The acoustic impedance across the foam growth surface is sufficient to prevent significant transmission of pressure oscillations from the foam above. This impedance barrier is created by the rapid change in gas-volume

fraction between the liquid and foam, which causes an acoustic velocity change of 2 orders of magnitude across the barrier.

Region 3 represents a section of the flow where the expanding foam is in contact with the tube wall. In this region the foam flows subject to the usual no-slip condition at a solid boundary. Pressure oscillations in region R3 display dominant frequencies in the range 10-30 Hz and may possibly contain lower frequencies based on visual observation of the pressure data (Plate 3-5). The interpretation of these oscillations is the same as our previous interpretation of unfragmenting flows, i.e., resonant longitudinal oscillation of the foam. The nonequilibrium acoustic velocity [Kieffer, 1977] calculated for gum rosin-organic solvent foam is between 10 and 15 m s^{-1} at gas-volume fractions ranging from 0.2 to 0.8. A 20 ± 5 Hz fundamental resonant frequency and resonator length of one half wavelength yields a foam column length of 0.2-0.5 m. These dimensions are less than the length of the unfragmented foam column (Plate 3 and 4), thus allowing for other flow regions to exist. Oscillations in the 80-100 Hz range are also observed (Plates 5-8), and we interpret these as weak radial oscillation modes in fashion similar to the unfragmenting flows.

Region R2 is subdivided into regions R2a and R2b. Image data (Plate 1) show that visible (0.5 cm and larger) gas pockets develop between the tube wall and the flowing foam in region R2b. These pockets then merge, giving rise to a foam-in-gas annular flow, that is the flow detaches from the tube wall, in region R2a. These two subregions are detectable by their pressure oscillation signatures (Plate 6 and Table 2) and are visible in images of the flows (Plate 1). As the foam passes from region R3 into R2b, there is a rapid change in the pressure oscillation behavior. In the acetone-driven flow the dominant frequency changes from 20 Hz in R3 to 80-100 Hz in R2b (Plate 6). In the ether-driven flow the passage of the fluid across this boundary is marked by the onset of more prominent 80-100 Hz peaks. The oscillation amplitude also increases by $\sim 50\%$ across this boundary. The foam then flows from R2b into R2a, and the pressure oscillation spectrum changes again, with an upfrequency broadening and the generation of some wave packets. This can be seen from the raw and band-passed pressure traces and the spectrograms in Plate 6. The 3-5 kPa oscillation amplitudes observed in R2a are the highest amplitudes observed in the flow field. We interpret the 80-100 Hz oscillations as radial modes that are now able to increase in amplitude because of the presence of gas at the interface between the foam and tube wall. The 20-Hz oscillations are considered to have the same origin as those detected in R3, i.e., a longitudinal resonant mode. The upfrequency broadening in R2a may be associated with a reduction in the diameter of the foam core or onset of different oscillation modes as separation from the wall becomes complete. The pressure gradient is greatest in region R2 (Plate 6), which is consistent with numerical simulations of volcanic conduit flows, indicating that the greatest pressure drop occurs across the fragmentation level or zone [Massol and Jaupart, 1999; Melnik, 2000].

Region R1 is defined by the presence of optically detected gas pockets (Plate 6), and the flow in this region consists of foam fragments dispersed in gas (Plate 1). A change in pressure oscillation behavior coincides with the optically detected gas pockets. The oscillations are complex and depend on the prevailing experimental conditions. It is also possible to subdivide region R1 on the basis of the pressure oscillation behavior (Plate 6 and Table 2). Region R1a shows very little spectral signal characterized by low or undetectable oscillations at all frequencies and rare wave packets. There are two types of spectra associated with these wave packets. Some are broadband, while others show evidence of a discrete range of frequencies in the 0.6-5 kHz band (e.g., at 0.52 s in Plate 6). Wave packets are particularly common in regions R1b and R2a, rarely present in

regions R1a and R2b, and never present in regions R3 and R4, that is, they are dominantly present when the flow is fully detached from the tube wall but still interacting with the wall on occasion. This implies that the wave packets could be due to direct impacts, or a stick-slip mechanism, between a foam slug and the nose of a pressure transducer. This process is more likely to cause broadband wave packets than a series of discrete frequencies. Another possibility is that the wave packets represent resonant oscillation of the gas between foam slugs. This process would likely manifest in a spectrum made of a series of narrowband peaks. Assuming a gas acoustic velocity of 240 m s^{-1} and a typical measured gas pocket length of 0.1 m , one obtains a fundamental frequency of 1.2 kHz , near the low end of the range of discrete frequencies observed (Plate 6). The series of observed resonant frequencies are complex and do not appear to be simple harmonic series.

5. Discussion of Experimental Observations

Our experimental observations suggest that nonerupting or effusive magmatic foam flows will generate low-frequency narrowband seismic signals whose frequencies are controlled by the conduit dimension and acoustic velocity of the fluid. Our observations also suggest that explosive eruptions generate low-frequency and relatively high-amplitude narrowband signals onto which higher-frequency broadband signals are superimposed.

The flow behaviors exhibited by vertical flows of boiling water and liquid metal range from bubbly through slug flow, to churn flow, to liquid-at-wall annular flow, to mist flow [Tong and Tang, 1997]. Gum rosin-organic solvent, hydrothermal, and magma-water systems are also examples of boiling flows. The gum rosin-organic solvent flow regimes range from bubbly/foam (zero velocity at wall) flow through detached (gas-pocket-at-wall and gas-at-wall annular) flow to coarse mist (fragmented) flow. Normal annular flow develops as gas bubbles concentrate at the central, high-velocity region of the flow in response to the Bernoulli effect [Tong and Tang, 1997]. A major fluid mechanical difference between these industrial and volcanic or analogue-volcanic systems is the viscosity of the liquid phase, which is much higher (and increasing) for both gum rosin and magma compared to water or liquid metals. This means that the relative motion of the bubbles and liquid is very small on the timescale of an explosive event, thereby preventing the development of a normal annular flow. As discussed in the next paragraph, the development of radial pressure gradients [Massol and Jaupart, 1999] with high pressure in the core of the flow is also likely to suppress the development of liquid-at-wall annular flow as this gradient favors higher gas-volume fractions at the tube wall and thus leads logically to the gas-at-wall annular flows observed here. Tong and Tang [1997] document one instance of formation of gas-at-wall, or inverted annular flow. This occurs when a subcooled liquid enters a hot section of tube that has a high heat flux. Gas is generated rapidly at the wall leading to an inverted annular flow. The liquid core is then broken up by the rapidly escaping gas in the annulus to form a mist flow. Illustrations of this type of flow bear striking phenomenological similarities to fragmenting gum rosin-organic solvent flows (Plate 1). Physical processes generating inverted annular flow in a low-viscosity boiling fluid are unlikely to be similar to those in either gum rosin-organic solvent or magma-water flows but may show similarity with hydrothermal systems. Two-liquid systems are known to segregate to produce core-annular flows [Carrigan and Eichelberger, 1990; Joseph and Renardy, 1992] with the low-viscosity liquid (e.g., mafic magma, water) migrating to the wall and enclosing a core of high-viscosity liquid (e.g., silicic magma, crude oil). The driving mechanism for this behavior is a minimization of viscous energy dissipation, which is achieved by having the low-viscosity liquid occupy the regions of highest

shear near the conduit wall. The gas-at-wall annular flow observed in region R2a in our experiment (Plate 8) has features similar to those observed in core-annular flows in that the flow is again organized with its lowest-viscosity component (the gas) at the wall so as to minimize viscous energy dissipation. However, the mechanism leading to this "lubricated" flow organization is obviously quite different in the foam-in-gas annular flow.

The physical mechanism for the development of gas pockets at the tube wall in our experiments underlies the eventual fragmentation of the foam and the generation of the mist, or fragmented flow. Insights into possible mechanisms are provided by the theoretical analysis of Massol and Jaupart [1999], who suggest that if the length scale over which a significant pressure change occurs is much smaller than the conduit length, then radial pressure gradients develop. These pressure gradients arise because under the assumption of Poiseuille flow in R3, the foam near the conduit walls is moving at a slower speed than that in the flow core. The foam close to the wall is therefore nearer equilibrium and more degassed with a higher liquid viscosity and gas-volume fraction. With less dissolved volatile, lower bubble pressures are maintained by the "old" foam near the tube walls than by the "fresh" foam in the flow core. The foam at the tube wall is therefore more non-Newtonian and permeable and will fail in a brittle fashion at lower strain rates than the foam in the flow core. This is especially so when viscosity is a strong function of volatile content, as in rhyolites and gum rosin (Figure 1). The Poiseuille flow breaks down upon entering R2, and the radial heterogeneities (gas-at-wall with foam core) and steep pressure gradient (Plate 6) in the R2 region of our experimental flows support the theoretical observation of radial pressure gradients having developed in R3. We suggest that the development of horizontal pressure gradients in R3 as viscosity increases because of degassing, especially at the tube wall, leads to a change in flow regime in R2 and ultimately to fragmentation in R1. Once an annular flow has developed and flow wall friction becomes effectively negligible, the foam core may be fragmented either by the high-velocity gas stream in the annulus as in rapidly heated boiling flow [Tong and Tang, 1997], or by vibrational, viscous, or viscoelastic instability of the foam core independent of the aerodynamic instability due to gas flow. If the experimental flows are considered to be similar to explosive volcanic flows, then a rapid sequence of flow regime changes from Poiseuille through bubble-at-wall and inverted annular to mist flow may be expected to underlie magma fragmentation also. In this case, the sequence of regime changes is considered to be generated by the development of radial pressure gradients as a consequence of rapid liquid viscosity increase [Massol and Jaupart, 1999]. If similarity is not considered close, then our experiments still demonstrate that a range of flow behavior richer than previously considered [e.g., Massol and Jaupart, 1999; Papale, 1999; Melnik, 2000] is likely to exist in explosive volcanic flows.

The pressure oscillation signatures documented here are distinctive enough to be used in the identification of flow regimes (Table 2). This suggests that different flow regimes identified within a fragmenting volcanic conduit flow may likewise generate different pressure oscillation signatures. Flow similarity between experimental and volcanic conduit flows suggests that the oscillatory behaviors should be similar. Pressure changes within a fluid-filled cavity will deform the solid bounding the cavity, and pressure oscillations within the cavity will radiate elastic waves within the confining medium [e.g., Aki et al., 1977; Ferrick and St. Lawrence, 1984; Chouet, 1985, 1986, 1992, 1996a]. These signals can be detected by seismometers and strain gauges. In experimental flows the pressure oscillations produce very small strains ($<10^{-5}$) in the confining tube. This is not the case in volcanic conduits that are kept open by the fluid pressure within them. If pressure oscillations with respect to average

pressure have similar amplitudes ($\Delta P/P$ up to 20%) in volcanic conduits as in experiments, then significant deformation of the confining medium is likely. There is an important difference between our experiments and volcanic systems in that there is no coupling between the elastic deformation of the conduit wall and the oscillating fluid in the experimental set-up. Nevertheless, the flow pressure oscillations measured in our experiments provide a baseline for comparisons with estimates of pressure fluctuations obtained from measurements of the ground response to volcanic activity.

6. Comparison With Seismic Observations in Volcanoes

Volcano seismic data may be qualitatively compared with our experimental pressure oscillations. Seismic data are complicated by path effects (e.g., low-pass filtering due to anelastic attenuation, and resonances in geologic structures) and difficulties in direct observation of the fluid mechanical processes taking place. Detailed correlation between seismoacoustic signals and surface activity is often difficult to achieve. The literature is dominated by observations of effusive and small-scale explosive activities that occur often and may be measured in relative safety. It is a general observation that seismic amplitudes increase, and the frequency range expands during explosive activity.

Chouet et al. [1997] showed that small discrete explosions superimposed on sustained tremor were the two persistent types of seismicity at Stromboli in April-May 1992. Sustained tremor and explosions could be distinguished from each other by their seismic signatures, suggesting that different fluid mechanical behaviors result in changes in seismic signals. The eruption of pyroclasts by bubble bursting was often accompanied by higher-frequency signals. This is qualitatively similar to the pressure oscillation behavior seen in the laboratory experiments reported here. Sustained 1.4-2.1 Hz tremor at Stromboli is present in a relatively static column of magmatic foam [*Chouet et al.* 1997], and sustained 10-30 Hz oscillations were observed in a relatively static gum rosin foam column in the experiment. *Chouet et al.* [1997] postulated that collective oscillations of bubbles ascending the magma conduit may provide sufficient energy for the self-excitation of tremor at Stromboli. This process may also be operating in our experiments with unfragmenting flows. *Chouet et al.* [1999] found two distinctive types of very long-period signals originating in two repetitive, nondestructive sources at Stromboli. Each waveform was associated with eruptions of different character from two vents that were fed from a common source region. These observations show that the broadband character of volcano seismic signals can yield information about subtle differences in vent geometries, as well as mechanisms of degassing taking place.

Sherburn et al. [1996] reported observations of harmonic tremor from White Island, New Zealand, where the fundamental and overtone frequencies remained stable for significant lengths of time when surface activity was low. When activity increased, producing an eruption column and generating shock waves, the tremor became nonharmonic, broadband and unstable and contained higher-frequency energy. On the basis of our experimental results we would attribute this behavior to rapidly changing dimensions and/or varying acoustic velocity of the magmatic cavity during explosive activity, both of which may have prevented the establishment of a stable resonator. We also surmise that the presence of higher frequencies indicates rapid changes in flow regime during explosive activity. The tremor source at White Island was attributed to bursting gas bubbles. However, the bubble-bursting mechanism thought to operate at White Island, and at Stromboli [*Ripepe et al.*, 1996], is unlikely

to be the cause of the oscillations seen in the experimental fragmenting flows.

McNutt [1987] found that major eruptions at Pavlov Volcano, Alaska, were accompanied by tremor episodes. The amplitude of the tremor signals scaled with eruptive explosivity, although the seismometer was often saturated during much of this explosive activity. Tremor amplitudes also scaled with lava fountain heights at Pavlov and Kilauea [*McNutt et al.*, 1991]. The same effect was demonstrated in experimental pressure oscillations, which were of small amplitudes in the nonfragmenting flows, and reached their largest amplitudes in region 2 of the fragmenting flows.

Effusive activity at Montserrat generated low-frequency, narrowband, and often monochromatic long-period events [*Neuberg et al.*, 1998]. These events preceded and accompanied rock falls and probably originated in fluid disturbances within the conduit or in fluid-filled cracks permeating the dome of Montserrat. This behavior is similar to the non-fragmenting experimental flows and the zero-velocity-at-wall region of the fragmenting flows.

Garcés et al. [1998] proposed that tremor signals observed at Arenal result from unsteady fluid flow during degassing. Following an explosion, an equilibrium magma column is perturbed. Acoustic and seismic data show that some time is then required for tremor to become established. This shows similarities to the experimental observations where oscillations are weak during the rapid growth phase of the unfragmenting flow (Figure 2 and Plate 2). At Arenal, fluid properties may have changed rapidly on the timescale of two oscillations, that is ≈ 2 s, effectively damping the establishment of a stable oscillator. At Arenal, 1-Hz tremor with several overtones eventually emerged from a broadband signal. This tremor is interpreted as a longitudinal resonance of the magmatic foam within the conduit.

Garcés et al. [1998] often found a lack of acoustic signals when the seismic signature of tremor was strong. They attributed this observation to the presence of a low acoustic velocity (high gas-volume fraction) magmatic foam acoustically decoupled from the resonating fluid column beneath it and isolating this column from the atmosphere. This mechanism is similar to that proposed for the absence of signals in the gas above the rapid growth stage of the nonfragmenting experimental flows (Figure 2 and Plate 2).

In our experiments the amplitudes of the pressure oscillations can be as high as 20% of the average pressure. Acoustic resonance in boiling water flows may have amplitudes that are "a significant fraction of the pressure level" [*Tong and Tang*, 1997, p. 464]. We can estimate the amplitude of pressure oscillations occurring during the February 1, 1996, volcanic crisis at Kilauea Volcano. The typical volume change associated with very long-period seismic signals recorded during this crisis was 3000 m^3 [*Ohminato et al.*, 1998]. Assuming a penny-shaped crack with radius of 200 m, we obtain an average wall opening $\langle w \rangle$ of 1.2 cm. Excess pressure may be estimated as $\Delta P = (5/4) (\pi \mu \langle w \rangle / R)$, where ΔP is the excess pressure, μ is the rigidity of the solid, and R is the crack radius [*Chouet*, 1985], with modification to account for the observed ratio of the P -to- S wave velocities in the source region [*Dawson et al.*, 1999], which implies the relationship between Lamé coefficients $\lambda = 4\mu$. Using $\mu = 7 \text{ GPa}$, we obtain $\Delta P = 1.6 \text{ MPa}$. The lithostatic pressure at the source depth of 1 km is 26.5 MPa, suggesting that the ratio of oscillation amplitude to average pressure is 6%. This value of $\Delta P/P$ for the February 1, 1996, volcanic crisis at Kilauea Volcano is about one third of the maximum value observed during our experiments.

Interpreting tilt signals preceding explosive eruptions at Sakurajima Volcano, Japan, on October 30 and November 14, 1986, *Uhira and Takeo* [1994] estimate values of excess pressure,

ΔP , of 0.5 MPa at a depth of 3.6 km below the crater floor. This would yield a $\Delta P/P$ of 0.5%. This value depends on the radius of the source of tilt, which was estimated to be 350 m [Uhira and Takeo, 1994]. If this value is too large, then the calculated $\Delta P/P$ will be correspondingly too small. Although the value of ΔP at Sakurajima is based on tilt data that may yield a ΔP significantly smaller than that associated with dynamic flow oscillations, it yields another rough estimate of the magnitude of pressure changes that may take place in a volcanic conduit. Given the uncertainties in obtaining reliable $\Delta P/P$ values for a wide range of volcanic eruption styles, the challenge in scaling our experimental results to natural volcanic conduit flows, and the difficulties in obtaining actual values of P for both experiments and volcanoes, we consider the coincidence between laboratory and field measurements to be an encouraging result.

7. Conclusions

The range of oscillatory behaviors measured in our experiments was correlated to the observed fluid flow regimes. Flow and acoustic similarities between experimental and volcanic conduit flows imply that unfragmenting magma foams should oscillate resonantly, with frequencies depending on length scales and acoustic velocities. The length scales are defined by the development of acoustic discontinuities at each end of the foam column and by conduit dimensions. The existence of such processes is strongly supported by the existing literature. Fragmenting flows display more complex oscillations. In general, an increase in amplitude and frequency broadening is common to both natural and laboratory explosive systems. Our experiments indicate that the bulk of the oscillatory energy is generated in the transition from zero-velocity-at-wall flow to fragmented flow as the flow is detaching from the wall and the foam core is breaking up. Our experiments and published theory [e.g., Melnik, 2000] show that this region is also subject to the steepest pressure gradient in the flow.

Surface observations and theoretical simulations of explosive volcanic eruptions suggest a range of conduit flow regimes. The gas-pocket-at-wall and gas-at-wall or inverted annular flows preceding fragmentation have not been previously reported in theoretical or experimental simulations of volcanic conduit flows. Radial flow heterogeneities associated with radial pressure gradients play a vital role in the onset of flow fragmentation in our experiments. This suggests that the neglect of radial pressure gradients in theoretical models is an inadequate assumption. The considerable radial heterogeneity occurring within these flows may have consequences for the transfer of acoustic energy to the conduit wall and the generation of seismic signals.

Each experimental flow regime has a characteristic pressure oscillation signature, suggesting that we may expect the same behavior from different flow regimes in a volcanic conduit flow even in the absence of system similarity. If the experimental and volcanic flows are similar, then these flow regimes and their pressure oscillations should also be similar. Experimentally, these pressure oscillations occur within expanding high-viscosity foam flows in parallel-sided smooth walled tubes. This suggests that pressure oscillations are a fundamental phenomenon associated with dynamic flow processes. Seismic observations of large-scale volcanic explosions are few. Seismoacoustic data from such eruptions would enable comparisons with our experimental system. The deployment of networks of high dynamic range broadband seismic instruments will be required to allow the observation of different flow regimes in volcanic conduit flows. Similarities between the ground response to volcanic conduit flow and oscillatory behavior observed in our experiments would provide strong evidence of flow similarity that is prerequisite to

translating seismic information into flow processes and modeling these processes.

Acknowledgments. S.J.L. acknowledges the Royal Society for travel grants to attend AGU and visit Menlo Park and for RSRG 15891 that funded much of this work. NERC is gratefully acknowledged for allowing part of grant GR9/01629 to be diverted into this research. We thank the LLNL for use of the SAC program. We are indebted to Claude Jaupart for discussions on similarities between our experimental foam flow behavior and those presented by *Massol and Jaupart* [1999]. We thank Julia Hammer, Charles R. Carrigan, Maggie Mangan, Jake Lowenstern, an anonymous reviewer, and AGU's editorial staff for greatly improving the manuscript.

References

- Aki, K., M. Fehler, and S. Das, Source mechanisms of volcanic tremor: Fluid-driven crack models and their application to the 1963 Kilauea eruption, *J. Volcanol. Geotherm. Res.*, **2**, 259-287, 1977.
- Benoit, J. P., and S. R. McNutt, New constraints on source processes of volcanic tremor at Arenal Volcano, Costa Rica, using broadband seismic data, *Geophys. Res. Lett.*, **24**, 449-452, 1997.
- Carrigan, C. R., and J. C. Eichelberger, Zoning of magmas by viscosity in volcanic conduits, *Nature*, **343**, 248-251, 1990.
- Chouet, B. A., Excitation of a buried magmatic pipe: A seismic source model for volcanic tremor, *J. Geophys. Res.*, **90**, 1881-1893, 1985.
- Chouet, B. A., Dynamics of a fluid-driven crack in three dimensions by the finite difference method, *J. Geophys. Res.*, **91**, 13,967-13,992, 1986.
- Chouet, B. A., Resonance of a fluid-driven crack: Radiation properties and implications for the source of long-period events and harmonic tremor, *J. Geophys. Res.*, **93**, 4375-4400, 1988.
- Chouet, B. A., A seismic model for the source of long-period events and harmonic tremor, in *IAVCEI Proceedings in Volcanology* edited by R. W. Johnson, G. Mahood and R. Scarpa, pp. 133-156, Springer-Verlag, New York, 1992.
- Chouet, B. A., Long-period volcano seismicity: Its source and use in eruption forecasting, *Nature*, **380**, 309-316, 1996a.
- Chouet, B. A., New methods and future trends in seismological volcano monitoring, in *Monitoring and Mitigation of Volcano Hazards*, edited by R. Scarpa and R. Tilling, pp. 23-97, Springer-Verlag, New York, 1996b.
- Chouet, B. A., R. A. Page, C. D. Stephens, J. C. Lahr, and J. A. Power, Precursory swarms of long-period events at Redoubt Volcano (1989-1990), Alaska: Their origin and use as a forecasting tool, *J. Volcanol. Geotherm. Res.*, **62**, 95-136, 1994.
- Chouet, B. A., G. Saccorotti, M. Martini, P. Dawson, G. De Luca, G. Milana, and R. Scarpa, Source and path effects in the wave fields of tremor and explosions at Stromboli Volcano, Italy, *J. Geophys. Res.*, **102**, 15,129-15,150, 1997.
- Chouet, B. A., G. Saccorotti, P. Dawson, M. Martini, R. Scarpa, G. De Luca, G. Milana, and M. Cattaneo, Broadband measurements of the sources of explosions at Stromboli Volcano, Italy, *Geophys. Res. Lett.*, **26**, 1937-1940, 1999.
- Cobbold, P. R., and M. P. A. Jackson, Gum rosin (colophony): A suitable material for thermomechanical modeling of the lithosphere, *Tectonophysics*, **210**, 255-271, 1992.
- Dawson, P. B., B. A. Chouet, P. B. Okubo, A. Villaseñor, and H. M. Benz, Three-dimensional velocity structure of the Kilauea caldera, Hawaii, *Geophys. Res. Lett.*, **26**, 2805-2808, 1999.
- Dingwell, D. B., Volcanic dilemma: Flow or blow?, *Science*, **273**, 1054-1055, 1996.
- Dingwell, D. B., and S. L. Webb, Structural relaxation in silicate melts and non-Newtonian melt rheology in geologic processes, *Phys. Chem. Miner.*, **16**, 508-516, 1989.
- Eichelberger, J. C., C. R. Carrigan, H. R. Westrich, and R. H. Price, Non-explosive silicic volcanism, *Nature*, **323**, 598-602, 1986.
- Ferrick, M. G., and W. F. St. Lawrence, Comment on "Observations of volcanic tremor at Mount St. Helens volcano" by Michael Fehler, *J. Geophys. Res.*, **89**, 6349-6350, 1984.
- Garcés, M. A., On the volcanic waveguide, *J. Geophys. Res.*, **102**, 22,547-22,564, 1997.

- Garcés, M. A., and R. A. Hansen, Waveform analysis of seismo-acoustic signals radiated during the fall 1996 eruption of Pavlof volcano, Alaska, *Geophys. Res. Lett.*, **25**, 1051-1054, 1998.
- Garcés, M. A., and S. R. McNutt, Theory of the airborne sound field generated in a resonant magma conduit, *J. Volcanol. Geotherm. Res.*, **78**, 155-178, 1997.
- Garcés, M. A., M. T. Hagerty, and S. Y. Schwartz, Magma acoustics and time-varying melt properties at Arenal Volcano, Costa Rica, *Geophys. Res. Lett.*, **25**, 2293-2296, 1998.
- Hammer, J. E., M. Manga, and K. V. Cashman, Non-equilibrium and unsteady fluid degassing during slow decompression, *Geophys. Res. Lett.*, **25**, 4565-4568, 1998.
- Harlow, D. H., J. A. Power, E. P. Laguerre, G. Ambubuyog, R. A. White, and R. P. Hoblitt, Precursory seismicity and forecasting of the June 15, 1991, eruption of Mount Pinatubo, in *Fire and Mud: Eruptions and Lahars of Mount Pinatubo, Philippines*, edited by C. G. Newhall and R. S. Punongbayan, 285-306, Univ. of Wash. Press, Seattle, 1996.
- Hess, K. U., and D. B. Dingwell, Viscosities of hydrous leucogranitic melts: A non-Arrhenian model. *Am. Mineral.*, **81**, 1297-1300, 1996.
- Howe, M. S., *Acoustics of Fluid-Structure Interactions*, Cambridge University Press, New York, 1998.
- Hurst, A. W., and S. Sherburn, Volcanic tremor at Ruapehu-Characteristics and implications for the resonant source, *N. Z. J. Geol. Geophys.*, **36**, 475-485, 1993.
- Jaupart, C., Physical models of volcanic eruptions, *Chem. Geol.*, **128**, 217-227, 1996.
- Jaupart, C., Gas loss from magma through conduit walls during eruption, in *The Physics of Explosive Volcanic Eruptions*, edited by J. S. Gilbert and R. S. J. Sparks, *Geol. Soc. Spec. Publ.*, **145**, 73-90, 1998.
- Jaupart, C., and S. Vergnolle, The generation and collapse of a foam layer at the roof of a basaltic magma chamber, *J. Fluid Mech.*, **203**, 347-380, 1989.
- Joseph, D. D., and Y. Y. Renardy, *Fundamentals of Two-Fluid dynamics, Interdisciplinary Appl. Math.*, vols. 3 and 4, Springer-Verlag, New York, 1992.
- Julian, B. R., Volcanic tremor: Nonlinear excitation by fluid flow, *J. Geophys. Res.*, **99**, 11,859-11,877, 1994.
- Kaminski, E., and C. Jaupart, The size distribution of pyroclasts and the fragmentation sequence in explosive volcanic eruptions, *J. Geophys. Res.*, **103**, 29,759-29,779, 1998.
- Kieffer, S. W., Sound speed in liquid-gas mixtures: Water-air and water-steam, *J. Geophys. Res.* **82**, 2895-2904, 1977.
- Kumagai, H., and B. A. Chouet, The complex frequencies of long-period seismic events as probes of fluid composition beneath volcanoes, *Geophys. J. Int.*, **138**, F7-F12, 1999.
- Kumagai, H., and B. A. Chouet, Acoustic properties of a crack containing magmatic or hydrothermal fluids, *J. Geophys. Res.*, **105**, 25,493-25,512, 2000.
- Leet, R. C., Saturated and subcooled hydrothermal boiling in groundwater flow channels as a source of harmonic tremor, *J. Geophys. Res.*, **93**, 4835-4849, 1988.
- Lu, N. Q., A. Prosperetti, and S. W. Yoon, Underwater noise emissions from bubble clouds, *IEEE J. Oceanic Eng.*, **15**, 275-281, 1990.
- Mader, H. M., E. Brodsky, D. Howard, and B. Sturtevant, Laboratory simulations of sustained volcanic eruptions, *Nature*, **388**, 462-464, 1997.
- Manga, M., J. Castro, K. V. Cashman, and M. Loewenberg, Rheology of bubble-bearing magmas, *J. Volcanol. Geotherm. Res.*, **87**, 15-28, 1998.
- Marti, J., C. Soriano, and D. B. Dingwell, Tube pumices as strain markers of the ductile-brittle transition during magma fragmentation, *Nature*, **402**, 650-653, 1999.
- Massol, H., and C. Jaupart, The generation of gas overpressure in volcanic eruptions, *Earth Planet. Sci. Lett.*, **166**, 57-70, 1999.
- Mayinger, F., Scaling and modelling laws in two phase flow and boiling heat transfer, in *Two-Phase Flow and Heat Transfer in the Power and Processing Industries*, Hemisphere, Washington, DC., 1981.
- McNutt, S. R., Observations and analysis of B-type earthquakes, explosions and volcanic tremor at Pavlof volcano, Alaska, *Bull. Seismol. Soc. Am.*, **76**, 153-175, 1986.
- McNutt, S. R., Eruption characteristics and cycles at Pavlof volcano, Alaska, and their relation to regional earthquake activity, *J. Volcanol. Geotherm. Res.*, **31**, 239-267, 1987.
- McNutt, S. R., T. P. Miller, and J. J. Taber, Geological and seismological evidence of increased explosivity during the 1986 eruptions of Pavlof volcano, Alaska, *Bull. Volcanol.*, **53**, 86-98, 1991.
- Melnik, O., Dynamics of two-phase conduit flow of high viscosity gas-saturated magma: large variations of sustained explosive eruption intensity, *Bull. Volcanol.*, **62**, 153-170, 2000.
- Morrissey, M. M., and B. A. Chouet, A numerical investigation of choked flow dynamics and its application to the triggering of long-period events at Redoubt volcano, Alaska, *J. Geophys. Res.*, **102**, 7965-7983, 1997a.
- Morrissey, M. M., and B. A. Chouet, Burst conditions of explosive volcanic eruptions recorded on microbarographs, *Science* **275**, 1290-1293, 1997b.
- Neuberg, J., B. Baptie, R. Luckett, and R. Stewart, Results from the broadband seismic network on Montserrat, *Geophys. Res. Lett.*, **25**, 3661-3664, 1998.
- Nishimura, T., and B. Chouet, Numerical simulations of seismic waves and magma dynamics excited by a volcanic eruption, *Eos Trans. AGU Fall Meet. Suppl.*, **79**(45), F595, 1998.
- Ohminato, T., B. A. Chouet, P. Dawson, and S. Kedar, Waveform inversion of very long period impulsive signals associated with magmatic injection beneath Kilauea volcano, Hawaii, *J. Geophys. Res.*, **103**, 23,839-23,862, 1998.
- Pandit, A. B., J. Varley, R. B. Thorpe, and J. F. Davidson, Measurement of bubble size distribution: An acoustic technique, *Chem. Eng. Sci.*, **47**, 1079-1089, 1992.
- Papale, P., Strain-induced magma fragmentation in explosive eruptions, *Nature*, **397**, 425-428, 1999.
- Phillips, J. C., S. J. Lane, A-M. Lejeune, and M. Hilton, A new experimental analogue system to investigate the dynamics of explosive volcanic eruptions, *Bull. Volcanol.*, **57**, 263-268, 1995.
- Prud'homme, R. K., and S. A. Khan, Experimental results on foam rheology in *Foams: Theory, Measurements and Applications*, edited by R. K. Prud'homme and S. A. Khan, 217-241, Marcel Dekker, New York, 1996.
- Ripepe, M., and E. Gordeev, Gas bubble dynamics model for shallow volcanic tremor at Stromboli, *J. Geophys. Res.*, **104**, 10,639-10,654, 1999.
- Ripepe, M., P. Poggi, T. Braun, and E. Gordeev, Infrasonic waves and volcanic tremor at Stromboli, *Geophys. Res. Lett.*, **23**, 181-184, 1996.
- Schindwein, V., J. Wassermann, and F. Scherbaum, Spectral-analysis of harmonic tremor signals at Mt-Semeru Volcano, Indonesia, *Geophys. Res. Lett.*, **22**, 1685-1688, 1995.
- Sherburn, S., B. J. Scott, and A. W. Hurst, Volcanic tremor and activity at White Island, New Zealand, July-September 1991, *N. Z. J. Geol. Geophys.*, **39**, 329-332, 1996.
- Sparks, R. S. J., M. I. Bursik, J. S. Gilbert, L. S. Glaze, H. Sigurdsson, and A. W. Woods, *Volcanic Plumes*, John Wiley, New York, 1997.
- Tong, L. S., and Y. S. Tang, *Boiling Heat Transfer and Two-Phase Flow*, Taylor and Francis, Philadelphia, Pa., 1997.
- Uhira, K., and M. Takeo, The source of explosive eruptions of Sakurajima Volcano, Japan, *J. Geophys. Res.* **99**, 17,775-17,789, 1994.
- Vergnolle, S., G. Brandeis, and J. C. Mareschal, Strombolian explosions, 2. Eruption dynamics determined from acoustic measurements, *J. Geophys. Res.*, **101**, 20,449-20,466, 1996.

B. A. Chouet and P. Dawson, Volcano Hazards Team, U.S. Geological Survey, 345 Middlefield Road, MS 910, Menlo Park, CA 94025. (chouet@chouet.wr.usgs.gov; dawson@pinatubo.wr.usgs.gov)

E. Hurst, S. J. Lane, and G. Ryan, Department of Environmental Science, Lancaster University, Lancaster LA1 4YQ, England, UK. (e.j.hurst@hotmail.com; s.lane@lancaster.ac.uk; g.ryan@lancaster.ac.uk)

J. C. Phillips, Centre for Environmental and Geophysical Flows, School of Mathematics, University of Bristol, University Walk, Bristol BS8 1TW, England, UK. (j.c.phillips@bristol.ac.uk)

(Received March 23, 2000; revised September 18, 2000; accepted October 9, 2000.)